Rend. Istit. Mat. Univ. Trieste
Vol. XXIX, 63–92 (1997)

Determining A Surface Breaking Crack From Steady-State Electrical Boundary Measurements – Reconstruction Method

C. Berenstein, D.-C. Chang and E. Wang (*)

Summary. - *We seek a non-destructive testing method to detect a radial surface breaking crack in a two-dimensional circular disk. The detection method utilizes steady-state electrical boundary measurements. A nonlinear function which characterizes the size and the location of a radial surface crack is constructed based on the knowledge of two data readings of the boundary voltage intensity corresponding to a current flux of dipole pattern. Based on this output function, we can detect the presence of a radial surface crack from two data readings of voltage intensity measurement on the boundary. And two convergent algorithms are derived individually to locate and then determine the size of the crack.*

(*) Authors' addresses: D.-C. Chang and E. Wang: Department of Mathematics, University of Maryland, College Park, MD 20742. C. Berenstein: Department of Mathematics, University of Maryland, College Park, MD 20742, and Institute for Systems Research, University of Maryland, College Park, MD 20742 (Japan).
1991 Mathematical Subject Classification: 35J25, 35Q80, 65H10, 65C20.
Key words: crack tip, crack length, flaw domains, analytic mappings, convergent algorithms.
Partially supported by NSF grant DMS 9622249.

1. Introduction

It is our purpose in this paper to explore a new Non-destructive Testing (NDT) procedure for crack detection by utilizing steady-state electrical field. The problem is approached through "parameterization". Namely, we assume the reference conductivity is known and parameterize "the unknown" in terms of the shapes, sizes, locations, and orientations of flaws. The term "parameterization" we are using here is adopted from many engineering references, *e.g.,* [5, 13, 20]. Among the applications of Inverse Problems to flaw detection, the concept of parameterization was first introduced by Friedman and Vogelius to determine an interior crack imbedded in a two-dimensional bounded domain [12]. Their idea was further extended to the case of multiple cracks [8]. Andrieux and Ben Abda later proposed a new reconstruction method for $2D$ or $3D$ domains to identify the plane which contains linear cracks [3]. Some computational algorithms have been proposed for flaw detection through parameterization approach. Based on a variation of Newton's method, Santosa and Vogelius constructed a computational algorithm to determine the location and the size of a linear crack which is imbedded in the interior of a two-dimensional, electrically conducting medium [18]. This method was extended in [9] to the case of multiple cracks. Their algorithms were further tested using lab data [16, 7]. These numerical studies all focused on detection of interior cracks. The case of surface breaking cracks was studied in [10, 10, 3]. All the works using parameterization approach so far assumed the shapes of probed cracks are priorly known.

We consider a two-dimensional geometry such that an inspected region is a circular disk with an accessible circumference, and a linear crack may tear from the circumference. We assume that the conductivity of the flawless disk is constant. For simplicity, the crack is further assumed to have the radial orientation. The current flux we shall apply to the probed region is a dipole pattern. To produce currents of dipole patterns, we attach a pair of source electrodes to the circumference in a way that the electrodes are placed at the endpoints of a diameter. DC currents (or AC currents at low frequency) are imported into the circular region through one of the electrodes and flow out of the area through the other electrode. For data collec-

tion, we measure and record the corresponding voltage field intensity along the circumference at the midpoints between the current source electrodes. In other words, each step of output measurement consists of two data readings from the corresponding voltage field intensity. We vary the locations of two input current electrodes around the circumference in the manner describe below so that each time the uncertainty of the location is reduced by half. Assume the reference conductivity is known, the goal is to determine whether a radial surface breaking crack exists in a circular region, and if it does, to reconstruct the crack from a finite number of boundary measurements.

Our reconstruction method comprises three stages:

(1) Identify a $2D$ damaged circular body from the flawless one.

(2) Locate the emerging tip of a surface breaking crack on the boundary.

(3) Determine the length of a surface breaking crack.

We will show that with the simple geometry of our model, it is possible to determine the length of a radial crack from only one single step of boundary measurement (which consists of two data readings of voltage field intensity) after the exterior crack tip is located. The work we present in this paper is the first part of our proposal of a fast and stable reconstruction method. Here we focus on the framework of the reconstruction method, including the ideas and the proofs for convergence of the algorithms. We will give detailed discussion about effectiveness and the the sensitivity property of the method in a forthcoming paper [6] (and also [19]).

Elcrat, Isakov, and Neculoiu proposed a computational method based on Schwartz-Christoffel transforms to detect one single surface breaking crack mainly in a polygonal domain [11]. The algorithm was extended to inspect collections of interior and surface breaking cracks in polygonal and doubly connected domains [10], where cracks simulated are also allowed to be piecewise linear and self intersecting. Our initial approach is similar to that used in [11, 10]. That is, we will employ an analytic transform to calculate voltage potential field in a flawed circular domain. However unlike the works in [11, 10],

the detection algorithms we propose have nothing at all to do with the computation of an analytic transform. We explicitly calculated voltage potential field by formulating an analytic mapping for our simpler geometry. The analytic mapping is used to observe and analyze only the boundary behavior of a voltage potential field in a flawed circular domain. Moreover, we will show that our numerical algorithms are convergent.

The method utilizes a nonlinear transcendental function of the crack parameters (location and length), which is constructed in terms of two data readings from voltage intensity measurement, and proved to be an increasing function of crack length. Based on this condition, we will show that the presence of a radial surface breaking crack is detectable by one single set of output measurements which consists of two data readings of the voltage field intensity corresponding to the same input current. The procedure to locate the emerging tip of a radial surface crack is based on the radial symmetry of our probed domains. It can be generalized to any radially symmetric geometry (e.g., annular cross section in the application to pipeline leakage). The algorithm to determine crack length involves solving the transcendental output equation for length parameter. We construct two iterative functions: *one is used to create a sequence of the lower bounds for crack length, the other is used to a sequence of the upper bounds for the crack length.* And we will show that the sequence of the upper bounds converges to the exact length of a radial surface crack. A different approach was also proposed to reconstruct a surface breaking crack [3]. Although their method provides a direct inversion formula and applies directly to more general geometry, they assumed the emerging tip of a surface breaking crack was a priori known. The results given in [3, 11, 10] all rely on the basic assumption that current and the corresponding voltage data are available on the *entire* boundary or a continuous part of the boundary (overspecified data). As we have mentioned in the preceding paragraph, we need only two data readings of the voltage intensity measurement corresponding to a current of dipole pattern to determine crack length in our case. In most of practical applications to probe a surface crack, we can always explicitly find conformal mappings to transform crack domains of more complicate

shapes to our model domain. Therefore, all the data measured in the original geometry can be transferred to the model of a circular disk via a suitable conformal mapping and processed using our algorithms. Therefore, one can set up an off-line table for an inspector to check up and compare real data with the corresponding measurements processed in the model of a circular disk. As implied by [11, 10], the computational cost for a conformal mapping is low. Due to the high speed and stability of our low-cost convergent algorithms (see [6, 19]), it is still worthy to apply our method to more complicated domains.

For other mathematical studies related to flaw detection, we refer the reader to [1, 2, 4, 14, 15].

The authors would like to thank the referee for many valuable suggestions of the paper.

2. The problem

Let $\Omega = \left\{x \in \mathbb{R}^2 \middle| 0 \leq |x| \leq r\right\}$ represent a circular conductor of radius r occupies and $\partial\Omega$ stand for its circumference. A crack will be denoted by σ. Under the assumptions of our model problem, σ is characterized by two parameters only: *the angular location of* σ, *denoted by* θ_σ, *and the crack length, denoted by* ℓ_σ. Consider the background medium is homogeneous except that the crack site is perfectly insulating. Without loss of generality, we assume the conductivity is equal to 1. Let P and Q stand for the locations of a pair of current electrodes. Then the steady-state voltage potential field, u, caused by a constant flux of dipole pattern , satisfies

$$\Delta u = \begin{cases} 0 & \text{in } \Omega \setminus \sigma, \\ \dfrac{\partial u}{\partial \nu} = 0 & \text{on } \sigma, \\ \dfrac{\partial u}{\partial \nu} = \delta_P - \delta_Q & \text{on } \partial\Omega, \end{cases} \tag{1}$$

where $\frac{\partial}{\partial \nu}$ denotes the unit outward normal derivative, and δ_x is the *Dirac distribution* which has concentrated intensity at the point $x \in \partial\Omega$.

We denote by $\frac{\partial}{\partial \tau}$ the counterclockwise tangential derivative along $\partial\Omega$. The voltage potential, u, modeled by (1) is not unique. It is

unique up to some constant. However, if we solve the direct problem (1) for u and calculate $\frac{\partial u}{\partial \tau}$ along $\partial\Omega$, we always obtain the unique presentation of the boundary measurement, $\frac{\partial u}{\partial \tau}$. Let f represent the distribution of $\frac{\partial u}{\partial \tau}$ along $\partial\Omega$, i.e.,

$$\frac{\partial u}{\partial \tau} = f \quad \text{on } \partial\Omega. \tag{2}$$

In the context of physics, the measurement, f, simply represents the corresponding voltage field intensity along $\partial\Omega$. If $\sigma \neq \varnothing$, then the extended line of σ divides the domain Ω into two half disks, say, Ω_1 and Ω_2. Let g represent the boundary measurement of the voltage potential associated with (1). Then

$$u|_{\partial\Omega} = (H_1 + H_2)g,$$

where H_1 and H_2 are functions of Heaviside-type defined on $\partial\Omega$ so that, for $j = 1, 2$,

$$H_j(x) = \begin{cases} 1, & \text{if } x \in \partial\Omega_j \\ 0, & \text{elsewhere.} \end{cases}$$

Even though $H_1 + H_2 = 1$ almost everywhere, but at the crack tip there is a discontinuity of the first kind. When we consider the weak derivative of the function $(H_1 + H_2)g$ with respect the τ variable, there will produce a δ function at the crack tip. It follows that the function f consists a δ term at the crack tip. From a theoretical aspect, it is not surprising that the tangential voltage field intensity across the exterior crack tip is mathematically characterized by the singularity due to a Dirac delta distribution. Hence, if one locates this singularity, then the exterior crack tip is identified. From the practical point of view, if the data of f is measured and collected near by the exterior crack tip, then when a probing head (designed to collect the data readings of f) moves across the crack, the presence of the singularity attributed to the δ term in f gives rise to a drastic fluctuation in the readings from a measuring device. And this fluctuation reflected on the data readings of f suffices to tell a crack investigator about the location of the exterior crack tip. While the preceding scenario in which f is measured close to the exterior crack tip is not quite troublesome and of particular interest to a

practical application, the major difficulty arises when the location of a surface breaking crack is unknown and the data of f happens to be collected away from the exterior crack tip. The question such as what should be the step to follow for next boundary measurement has been an open question in NDT subject for engineers. It is therefore worthwhile to explore an efficient and stable algorithm to locate a neighborhood which is close to the exterior crack tip even that the method does not serve as a closed formula to identify the singularity of the resulting voltage potential. Our effort in this paper to locate a surface breaking crack is firmly based on this standpoint. It is also for this reason that in our work, we always assume that the data of f are to be measured and collected away from the exterior crack tip in the presence of a surface breaking crack.

Given an input current flux of dipole pattern, we assume the data of f measured on the boundary are accessible. Each single set of output measurements will contain two data readings of f. Whenever a surface breaking crack is present in Ω, the source electrodes at P and Q always divide $\partial\Omega$ into two arcs (assuming P and Q are located away from σ) : one arc is flawless and the other represents the damaged part where σ penetrates $\partial\Omega$. Denote by M the midpoint between P and Q on the flawless arc and by M_σ the other midpoint on the damaged part. In case the probed region is perfect without any defect, symbolically we replace the notation, M_0, for M_σ. In particular, we choose P and Q to be at the endpoints of some diameter of Ω. The diameter joining P and Q will be referred to as the *"current diameter"* (Fig. 1). In the following paragraphs, if an upper case letter represents a point, then the corresponding lower case letter denotes the angular location of the point (e.g., the angular location of P will be denoted by p, and the angular location of M_σ will be denoted by m_σ, etc.).

3. The main results

3.1 Determining the presence of a surface breaking crack

We give a simple condition to determine whether a radial surface breaking crack exists in Ω. We first transform the crack domain $\Omega \setminus \sigma$ into the unit disk via an explicit analytic mapping. Then we

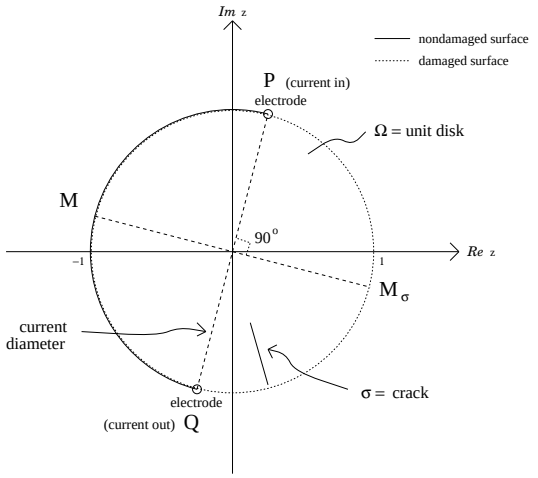

Fig. 1

solve the corresponding equations to the PDEs (1) for the voltage potential field on the unit disk. In this way we can formulate f in terms of crack parameters $(\ell_\sigma, \theta_\sigma)$ and the locations for voltage boundary measurements. Fig. 2 and Fig. 3 show that the global distribution of f along $\partial\Omega$ of a damaged domain is different from that of a flawless domain. We will show that the presence of such a crack is detectable by two data readings of the voltage field intensity corresponding to the same input current.

We first construct an output function in terms of the boundary measurement of voltage field intensity. Let s be the ratio of the crack length ℓ_σ to the radius r of Ω. That is

$$s = \frac{\ell_\sigma}{r}, \tag{3}$$

We call s the *relative crack length*. Thus, $s = 0$ if the probed conductor is flawless. We take the ratio of voltage field intensity at M to that at M_σ. This ratio is proved to be increasing with the relative crack length, s, for an arbitrarily fixed current diameter. So we

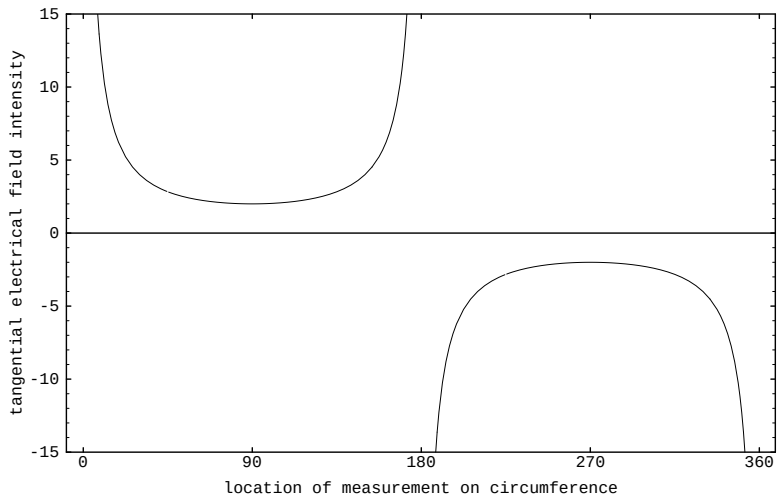

Fig. 2: The electrical field intensity along the circumference of a flawless disk. The horizontal axis displays the angular location (in degrees) of the boundary measurement. P is located at 180°, and Q is located at 0°.

define

$$\gamma_{p-\theta_\sigma}(s) := \frac{f \text{ at } M}{f \text{ at } M_\sigma}, \quad p-\theta_\sigma \neq n\pi, (n+\frac{1}{2})\pi, \quad n \in \mathbb{Z}, \tag{4}$$

where the subscripts $p-\theta_\sigma$ indicates that the ratio function depends on $p-\theta_\sigma$, the angle between the current diameter and the crack. We have the following result.

THEOREM 3.1. *Suppose $p-\theta_\sigma \neq n\pi, (n+\frac{1}{2})\pi$, $n \in \mathbb{Z}$. Then $\gamma_{p-\theta_\sigma}(s)$ is an increasing function of s for $0 \leq s < 2$. Moreover,*

$$\gamma_{p-\theta_\sigma}(s) = 1 + \eta_{p-\theta_\sigma}(s) \cdot s, \quad 0 \leq s < 2, \tag{5}$$

where $\eta_{p-\theta_\sigma}(s) \geq 0$, is a continuous function of s for $0 \leq s < 2$. The subscript $p-\theta_\sigma$ indicates $\eta_{p-\theta_\sigma}$ depends on the value of $p-\theta_\sigma$. We also have the following estimate for $\eta_{p-\theta_\sigma}(s)$:

$$\eta_{p-\theta_\sigma}(s) \leq \frac{s}{(2-s)^2} \cdot \alpha_{p-\theta_\sigma}(s_b), \quad \text{for} \quad 0 < s < s_b < 2. \tag{6}$$

where $\alpha_{p-\theta_\sigma}$ is given in (39), Appendix.

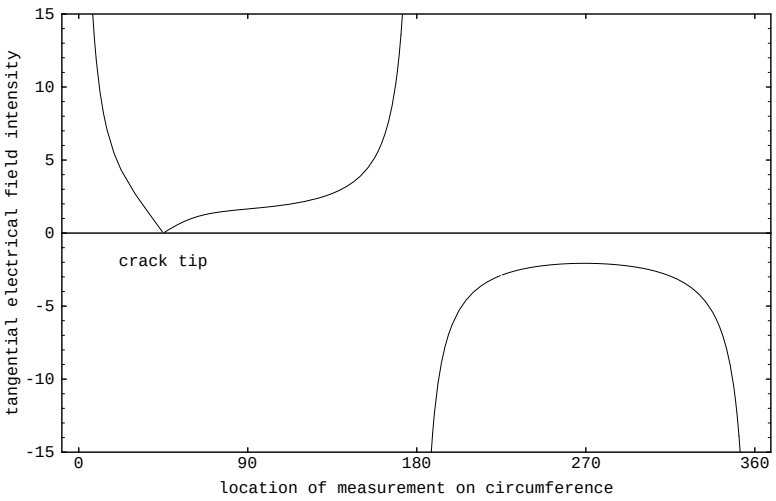

Fig. 3: The electrical field intensity along the circumference of a damaged disk. The horizontal axis displays the angular location (in degrees) of the boundary measurement. The crack penetrates the boundary at 45°.

Proof. Without loss of generality, we assume Ω = the unit disk = $\{z \in \mathbb{C} \mid |z| < 1\}$. Hence $\ell_\sigma = s$ by (3). First, we prove the case that σ lies on the positive real axis. Let

$$\tilde{h}_\sigma(z) = \frac{i - \left(\left(\frac{s}{2-s}\right)^2 - \left(\frac{z-1}{z+1}\right)^2\right)^{1/2}}{i + \left(\left(\frac{s}{2-s}\right)^2 - \left(\frac{z-1}{z+1}\right)^2\right)^{1/2}},$$

where we consider the branch $\{z \in \mathbb{C} \mid 0 < \arg(z) < 2\pi\}$ whenever the square root is involved. Then $\tilde{h}_\sigma(z)$ is a one-to-one analytic mapping from $\Omega \setminus \sigma$ onto $\{z \in \mathbb{C} \mid |z| < 1\}$. To solve the boundary value problem (1), we need consider a topological extension of $\tilde{h}_\sigma(z)$ to the closure of $\Omega \setminus \sigma$. So let us define

$$\begin{aligned} \Omega^+ &= \Omega \cap \mathbb{R}^2_+, \\ \Omega^- &= \Omega \cap \mathbb{R}^2_-, \\ \partial\Omega^+ &= \partial\Omega \cap \mathbb{R}^2_+, \quad \text{and} \quad \partial\Omega^- = \partial\Omega \cap \mathbb{R}^2_-. \end{aligned}$$

Regarding σ as a double-edged slit, the upper edge is denoted by σ^+ and the lower part by σ^-. Thus $\sigma = \sigma^+ \cup \sigma^-$. Define $h_\sigma : \overline{\Omega \setminus \sigma} \to \overline{\Omega}$

to be

$$h_\sigma(z) := \begin{cases} \tilde{h}_\sigma(z) & \text{for} \quad z \in \Omega \setminus \sigma, \\ \lim\limits_{\Omega^+ \ni z_n \to z} \tilde{h}_\sigma(z_n) & \text{for} \quad z \in \partial\Omega^+ \cup \sigma^+, \\ \lim\limits_{\Omega^- \ni z_n \to z} \tilde{h}_\sigma(z_n) & \text{for} \quad z \in \partial\Omega^- \cup \sigma^-. \end{cases}$$

Then h_σ is a topological map of $\tilde{h}_\sigma$ extended to the closure of $\Omega \setminus \sigma$.

The above calculation is based on the assumption that $\theta_\sigma = 0$. To calculate an analytic mapping h_σ for the case $\theta_\sigma \neq 0$, we first rotate $\Omega \setminus \sigma$ clockwise through an angle of θ_σ, so that σ lies on the positive real axis. The effect of this rotation on h_σ is equivalent to translation by $-\theta_\sigma$ units on the factor K_s throughout the entire course of calculations (The expression of K_s is given in (33), Appendix).

Let $G(\cdot,\cdot)$ represent the Green's function for the Neumann Problem in the unit disk. Since the Green's function for the Laplacian is conformally invariant, hence the solution to (1) can be written as

$$u(z) = G\big(h_\sigma(P), h_\sigma(z)\big) - G\big(h_\sigma(Q), h_\sigma(z)\big), \qquad z \in \Omega \setminus \sigma.$$

By definition (4) and in polar coordinates, we can express $\gamma_{p-\theta_\sigma}(s)$ in terms of the angular locations of boundary data (represented by the input-output parameters p, q, m, and m_σ) and the crack parameters (represented by the variables θ_σ and s. See (32), Appendix).

We decompose the expression of $\gamma_{p-\theta_\sigma}(s)$ into the product of the following factors,

$$\gamma_{p-\theta_\sigma}(s) = A_{p-\theta_\sigma}(s) \cdot B_{p-\theta_\sigma}(s) \cdot C_{p-\theta_\sigma}(s) \cdot D_{p-\theta_\sigma}, \tag{7}$$

where $A_{p-\theta_\sigma}(s)$, $B_{p-\theta_\sigma}(s)$, $C_{p-\theta_\sigma}(s)$, and $D_{p-\theta_\sigma}$ are defined in (34) – (37), Appendix. Since $\gamma_{p-\theta_\sigma}(0) = 1$, the results (5) and (6) follows by plugging into (7) Taylor's expansions of $A_{p-\theta_\sigma}(s)$, $B_{p-\theta_\sigma}(s)$, and $C_{p-\theta_\sigma}(s)$ around 0. □

REMARK 3.2. According to the discussion in the paragraph after equation (2), one should understand that it is not in the authors' concern to define as well as interpret the γ function given in (4) suppose the point M_σ happens to be z_σ, the exterior crack tip (in which $p-\theta_\sigma = (n+1/2)\pi$). We also realized that Fig. 3 does not completely

represent the distribution of the voltage intensity along the boundary of a crack domain, mainly because of the limitation to the graphic tool we used prohibited to plot a blow-up phenomenon at a single point. Nevertheless, we still present this plot since it demonstrates obviously unequal distributions of the boundary voltage intensity in two half disks divided by a crack.

The increasing phenomenon of $\gamma_{p-\theta_\sigma}$ with crack length is demonstrated in Fig. 4 for a particular case. Different angles between a current diameter and the probed crack determine different variations of the curve for $\gamma_{p-\theta_\sigma}$ (Fig. 5). Since (5) implies that $\gamma_{p-\theta_\sigma}(s) = 1$ if $s = 0$ and $\gamma_{p-\theta_\sigma}(s) > 1$ if $s > 0$, by definition (4), we obtain the following result.

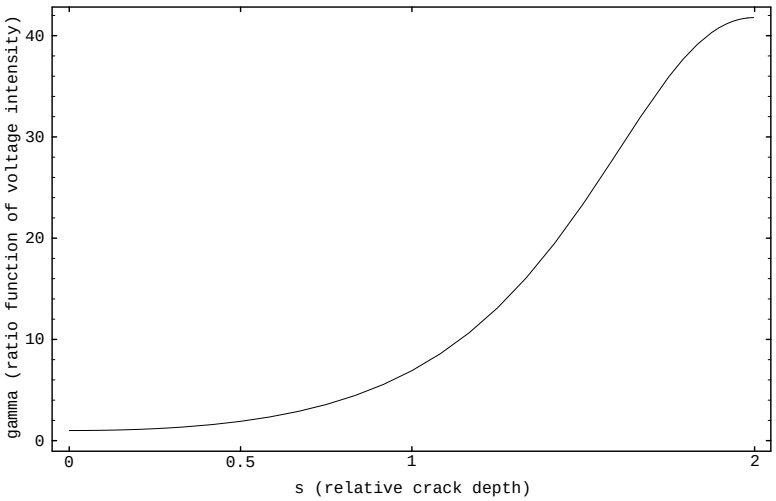

Fig. 4: $\gamma_{p-\theta_\sigma}(s)$ increases with s when $p - \theta_\sigma = 60°$.

THEOREM 3.3. (Determining the presence of a radial surface breaking crack). *Arbitrarily choose a current diameter and build up a current loop between the endpoints (P and Q) of the diameter. Then*

(1) the voltage field intensities at M and M_σ are equal if there is no crack in Ω, otherwise,

(2) the voltage field intensity at M is larger than that at M_σ if a radial surface breaking crack is present in Ω.

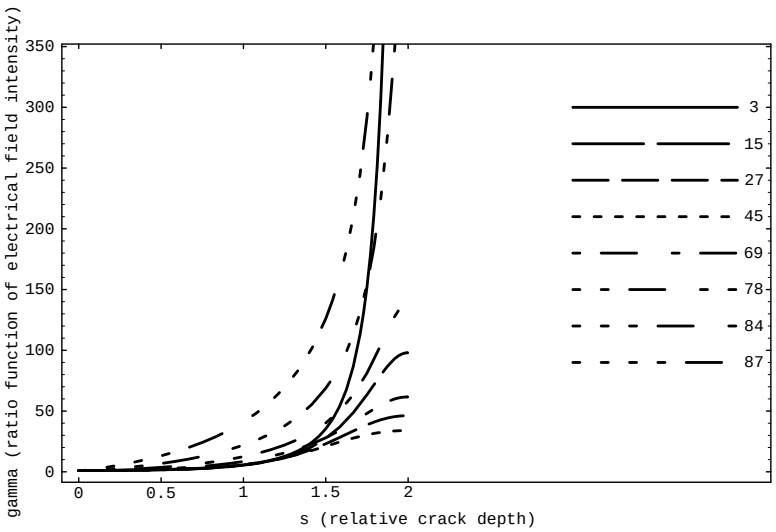

Fig. 5: The curves of $\gamma_{p-\theta_\sigma}(s)$ associated with different angles between the current diameter and the crack. The number appended to the curve indicate the associated value of $p-\theta_\sigma$ which is measured in degrees. $\gamma_{p-\theta_\sigma}(s)$ is increasing with s.

REMARK 3.4. The preceding considerations are all based on the assumption (4) that $p-\theta_\sigma \neq n\pi, \left(n+\frac{1}{2}\right)\pi$. Here the authors applied the topological extension of an analytic map from the crack domain onto a unit disk to calculate the resulting voltage potential field in the crack domain. In these calculations, the crack domain is considered as a Riemann surface with a cut (or a double-edged slit). As long as one electrode (say P) is placed on z_σ in the sense that $P \to z_\sigma$ from either side of the crack (this could happen in a real application when the electrode is not riding across the crack and hence not in contact with two sides of the surface around the crack at the same time), the resulting measurements are never the same as those in the flawless case. This is confirmed in the more detailed calculations of f (see [19]). Suppose one input electrode (say P) is riding over z_σ (in practice with the electrode touching the surface on two sides of the crack), then $\gamma_{p-\theta_\sigma} = 1$ due to the symmetry of the reference geometry. If this condition occurs, an inspector can always move the electrodes a little bit away from the original locations and take one more measurement. The new action should be sufficient to determine

the presence of a radial surface breaking crack. Again from the practical point of view, the situation in which one electrode happens to be riding over z_σ does not give rise to a mysterious scenario. Therefore, we will not be bothered to analyze this case. Instead, the authors are more interested in the cases that the input electrodes are placed away from the crack and hence always assume that $p - \theta_\sigma \neq n\pi$.

3.2 Determining the flaw site

Theorem 3.3 enables us to distinguish a damaged domain from a flawless domain. To locate the flaw site, we introduce a procedure called *trapping strategy*. The idea is to generate a sequence of searching regions, all of which contain the crack. The searching region gets smaller and smaller until eventually trap the crack at tie right location. The principle we apply rests on Theorem 3.3 (2).

We start with the entire domain, Ω. When $\sigma \neq \varnothing$, any arbitrarily chosen current diameter divides Ω into two half disks : *one of the half disks is flawless and the other contains* σ. Let us denote the damaged half disk by D_1 (Fig. 6, $j = 1$). Theorem 3.3 (2) implies that D_1 must be the half disk containing M_σ at which the smaller voltage field intensity is measured. Thus, we narrow down searching region from the entire domain to the half disk, D_1. For the second step of measurement, we rotate the current diameter so that it divides D_1 into two quarters of Ω. Let D_2 stand for the damaged quarter so that $\sigma \in D_2$ (Fig. 6, $j = 2$). How do we distinguish D_2 from the other flawless quarter ? Note that the new current diameter also divides Ω into one flawless half disk and the other damaged half, say $D_1{}'$. So $\sigma \in D_1{}'$. Similarly, $D_1{}'$ can be determined by applying Theorem 3.3 (2). We observe that (Fig. 6, $j = 2$)

$$D_2 = D_1 \cap D_1{}'.$$

Therefore, we have further narrowed down searching region from the half disk D_1 to the quarter disk D_2. To obtain a even smaller searching region than D_2, we rotate the current diameter to a position so that it equally divides D_2 into two sectors: *one is flawless and the other, say* D_3, *contains* σ (Fig. 6, $j = 3$). Applying Theorem 3.3 (2), we can similarly locate D_3. If we continue with this format of

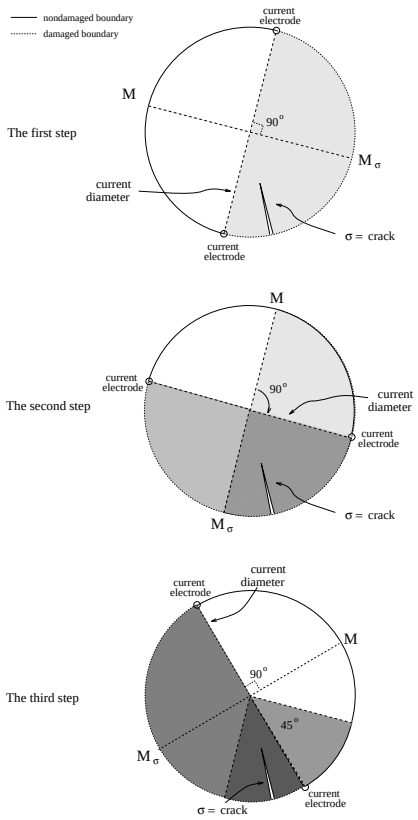

Fig. 6: Demonstration of *trapping strategy.*

bisecting process, we will obtain a sequence of flaw regions : D_1, D_2, D_3, $\cdots$. The sequence has the following nesting relation:

$$D_1 \supset D_2 \supset D_3 \supset \cdots \supset \sigma.$$

Moreover, we can estimate the exact size of each of these flaw regions:

$$\text{The area of } D_j = \frac{1}{2^j} \text{ of } \Omega, \quad j = 1, 2, 3, \cdots .$$

The physics for each step of measurement is modeled by the following PDEs associated with a set of different dipole locations, $\{P_j, Q_j\}$

which are away from σ:

$$\begin{aligned} \Delta w_j &= 0 && \text{in} \quad \Omega \setminus \sigma, \\ \frac{\partial w_j}{\partial \nu} &= 0 && \text{on} \quad \sigma, \\ \frac{\partial w_j}{\partial \nu} &= \delta_{P_j} - \delta_{Q_j} && \text{on} \quad \partial\Omega, \quad j = 1, 2, \cdots, \end{aligned} \tag{8}$$

and let

$$f_j = \frac{\partial w_j}{\partial \tau}\bigg|_{\partial\Omega}, \qquad j = 1, 2, \cdots. \tag{9}$$

For each j, let R_j denote the midpoint of $\overset{\frown}{P_j Q_j}$, which stands for the curve that one traverses from P to Q along $\partial\Omega$ counterclockwise. And let N_j denote the midpoint of $\overset{\frown}{Q_j P_j}$. The algorithm will quantitize the rotational angle of the current diameter, $\overline{P_j Q_j}$, for each step of measurement. It also provides a simple rule of rotation in terms of clockwise or counterclockwise direction without regard to the location of each searching region D_j.

THEOREM 3.5. (A convergent algorithm to locate exterior crack tip). *Let z_σ denote the location of the exterior crack tip. A pair of dipole locations, $\{P_0, Q_0\}$, are arbitrarily chosen so that $|p_0 - q_0| = \pi$. For $j = 0, 1, 2, ...$, P_j and Q_j are determined by the following conditions:*

(1) If $\left|f_j(r_j)\right| > \left|f_j(n_j)\right|$, then rotate P_j and Q_j counterclockwise along $\partial\Omega$ through an angle of $\frac{\pi}{2^{j+1}}$ to obtain P_{j+1} and Q_{j+1} respectively.

(2) If $\left|f_j(r_j)\right| < \left|f_j(n_j)\right|$, then rotate P_j and Q_j clockwise along $\partial\Omega$ through an angle of $\frac{\pi}{2^{j+1}}$ to obtain P_{j+1} and Q_{j+1} respectively.

Then

$$Q_j \to z_\sigma, \qquad \text{as} \quad j \to \infty.$$

Moreover,

$$\measuredangle Q_j O z_\sigma \leq \frac{\pi}{2^j}, \qquad \forall j = 0, 1, 2, \cdots,$$

where O is the center of Ω and $\measuredangle WYZ$ stands for the acute angular measurement of an angle $\angle WYZ$.

Proof. By induction. □

3.3 Determining crack length

By solving the direct problem (1), we have expressed $\gamma_{p-\theta_\sigma}(s)$ in terms of the angular locations of boundary data (represented by the parameters p, q, m, and m_σ), and the crack parameters (represented by the variables θ_σ and s). Under the restriction $0° < p - \theta_\sigma < 90°$, we obtain a nonlinear equation

$$\text{measured data} = \frac{\text{voltage field intensity at M}}{\text{voltage field intensity at } M_\sigma} = \gamma_{p-\theta_\sigma}(s). \quad (10)$$

The expression of $\gamma_{p-\theta_\sigma}(s)$ is lengthy, so we present it in the appendix.

After locating the emerging tip of a crack, all the variables in (10) are known except for s. There is no obvious way to solve (10) for s in terms of a closed formula. For that reason, we introduce an iterative algorithm to estimate s. The idea is to employ *radial damage size growth limit* (see [17] for the definition) or any possible upper bound of exact crack length as an initial guess, and create a sequence of length estimates so that the sequence of the length estimates converges to the actual crack length.

First, we would like to point out that given an priori upper bound of s, it is always possible to find a lower bound for s in terms of the output measurement, $\gamma_{p-\theta_\sigma}(s)$. The statement is presented in the following lemma.

LEMMA 3.6. (Finding a lower bound of s from an existing upper bound). *Suppose* $0 < s < s_b < 2$. *Then*

$$s > 2\sqrt{\frac{\gamma_{p-\theta_\sigma}(s)-1}{\alpha_{p-\theta_\sigma}(s_b)}}\Bigg/\left(1+\sqrt{\frac{\gamma_{p-\theta_\sigma}(s)-1}{\alpha_{p-\theta_\sigma}(s_b)}}\right) > 0 \quad (11)$$

for $0 < p - \theta_\sigma \leq \pi/2$, *where the expression of* $\alpha_{p-\theta_\sigma}(\cdot)$ *is given in (39), Appendix.*

Proof. Substituting (6) into (5) and solving the resulting inequality for s, the first inequality follows. The second inequality follows immediately since $\gamma_{p-\theta_\sigma}(s) > 1$ by (5). □

Based on the foregoing lemma, we now construct a lower bound function for relative crack length as follows

$$\lambda_{p-\theta_\sigma}(y) = 2\sqrt{\frac{\gamma_{p-\theta_\sigma}(s)-1}{\alpha_{p-\theta_\sigma}(y)}}\Bigg/\left(1+\sqrt{\frac{\gamma_{p-\theta_\sigma}(s)-1}{\alpha_{p-\theta_\sigma}(y)}}\right), \qquad (12)$$

It is easy to show that $\lambda_{p-\theta_\sigma}(\cdot)$ is decreasing on $[0,2)$ for any fixed p and θ_σ.

Next step of our approach is to show that with the knowledge of an upper bound and also a lower bound of s, we can find a smaller upper bound for s in terms of the output measurement, $\gamma_{p-\theta_\sigma}(s)$. To this point, we recall that $A_{p-\theta_\sigma}(s)$, $B_{p-\theta_\sigma}(s)$, $C_{p-\theta_\sigma}(s)$, and $D_{p-\theta_\sigma}$ have been defined in (34) – (37). $\phi_{j,p-\theta_\sigma}(x,y)$ $(j=1,2,3)$ is given in (40) (Appendix). Let s_{lb} and s_b be two positive numbers such that $s_{lb} \le s < s_b$. Denote

$$\begin{cases} A = A_{p-\theta_\sigma}(s_b), \\ B = B_{p-\theta_\sigma}(s_b), \\ C = C_{p-\theta_\sigma}(s_b), \\ D = D_{p-\theta_\sigma}, \end{cases}$$

and let

$$\Phi_j = \phi_{j,p-\theta_\sigma}(s_{lb}, s_b), \quad \text{j = 1,2,3.}$$

The following two lemmas hold under the condition $s_{lb} \le s < s_b$.

LEMMA 3.7. *Assume* $0 < p-\theta_\sigma < \pi/2$, *and* $0 < s_b \le 1$. *Then*

$$s < s_b - \frac{\gamma_{p-\theta_\sigma}(s_b) - \gamma_{p-\theta_\sigma}(s)}{\beta_{p-\theta_\sigma}(s_{lb}, s_b)}$$

if $s \ge \max\left\{s_b - \frac{A}{\Phi_1}, s_b - \frac{B}{\Phi_2}, s_b - \frac{C}{\Phi_3}\right\}$.

Proof. Take Taylor's expansions of $A_{p-\theta_\sigma}(s)$, $B_{p-\theta_\sigma}(s)$, and $C_{p-\theta_\sigma}(s)$ around s_b. The rest of the argument is slightly different but similar to the proof of the estimate (6). □

LEMMA 3.8. $\beta_{p-\theta_\sigma}(\cdot,\cdot)$ *is defined in (41). Let* s_{lb} *and* s_b *be two positive numbers so that* $s_{lb} \le s < s_b$. *Assume* $0 < p-\theta_\sigma < \pi/2$ *and* $1 < s_b < 2$. *Then*

(1) for $s \geq s_b - 1$,

$$s < s_b - \frac{\gamma_{p-\theta_\sigma}(s_b) - \gamma_{p-\theta_\sigma}(s)}{\beta_{p-\theta_\sigma}(\tilde{s}_{lb}, s_b)},$$

if $s \geq \max\left\{s_b - \frac{A}{\widetilde{\Phi}_1}, s_b - \frac{B}{\widetilde{\Phi}_2}, s_b - \frac{C}{\widetilde{\Phi}_3}\right\}$, *where* $\tilde{s}_{lb} = \max(s_{lb}, s_b - 1)$, *and*

$$\widetilde{\Phi}_j = \phi_{j,p-\theta_\sigma}(\tilde{s}_{lb}, s_b), \quad \text{j} = 1,2,3.$$

(2) for $s < s_b - 1$,

$$s < \min\left(s_b - 1, \sqrt[3]{\frac{\gamma_{p-\theta_\sigma}(s_b) - \gamma_{p-\theta_\sigma}(s)}{\beta_{p-\theta_\sigma}(s_{lb}, s_b)}}\right).$$

if $s \geq \max\left\{s_b - \frac{A}{\Phi_1}, s_b - \frac{B}{\Phi_2}, s_b - \frac{C}{\Phi_3}\right\}$.

Proof. Analogous to the proof of Lemma 3.7. □

Based on Lemma 3.7 and Lemma 3.8, we obtain the following result.

LEMMA 3.9. (Finding a smaller upper bound for s from an existing pair of lower bound and an upper bound). *Assume* $0 < p - \theta_\sigma < \pi/2$. *Let* s_{lb} *and* s_b *be two positive numbers so that* $s_{lb} \leq s < s_b$. *Then*

$$s < \omega_{1,p-\theta_\sigma}(s_{lb}, s_b) \leq s_b \tag{13}$$

if $\gamma_{p-\theta_\sigma}(s) \geq \gamma_{p-\theta_\sigma}\big(\omega_{2,p-\theta_\sigma}(s_{lb}, s_b)\big)$ *or* $\omega_{2,p-\theta_\sigma}(s_{lb}, s_b) < 0$, *where* $\omega_{1,p-\theta_\sigma}$ *and* $\omega_{2,p-\theta_\sigma}$, *defined in (42) – (43) (Appendix), are constructed from the output measurement,* $\gamma_{p-\theta_\sigma}(s)$, *and all the known parameters.*

The principle behind the construction of the length algorithm rests on Lemma 3.6 and Lemma 3.9. With the knowledge of an upper bound, s_b, as an initial guess for s, Lemma 3.6 implies that we can find a nonzero lower bound, s_{lb}, so that s is trapped in the interval $[s_{lb}, s_b]$. Then applying Lemma 3.9, we further reduce the upper bound from s_b to the value given by $\omega_{1,p-\theta_\sigma}(s_{lb}, s_b)$ under a specific condition given in the lemma. If we update the assumed

upper bound of s to be $\omega_{1,p-\theta_\sigma}(s_{lb}, s_b)$, by applying Lemma 3.6 again, we then generate a new lower bound for s. It is our hope that the new lower bound is larger than the former lower bound, s_{lb}, so that we obtain a smaller trapping interval for s. We also hope that by recursively applying Lemma 3.9 and Lemma 3.6, we are able to generate an increasing sequence of lower bounds and a decreasing sequence of upper bounds for s.

Now, we come to the main body of our length reconstruction algorithm. For any particular choice of the location on the circumference to import a current flux, or say, given any fixed value of p, we construct two iterative functions as follows:

$$\lambda_{p-\theta_\sigma}(y) = 2\sqrt{\frac{\gamma_{p-\theta_\sigma}(s)-1}{\alpha_{p-\theta_\sigma}(y)}}\Bigg/\left(1+\sqrt{\frac{\gamma_{p-\theta_\sigma}(s)-1}{\alpha_{p-\theta_\sigma}(y)}}\right), \tag{14}$$

where the expression for $\alpha_{p-\theta_\sigma}(y)$ is given in (39) (see Appendix). $\gamma_{p-\theta_\sigma}(s)$ has to be replaced by the boundary data measured from the corresponding voltage field intensity (10). Also

$$\omega_{p-\theta_\sigma}(x,y) = \begin{cases} \omega_{1,p-\theta_\sigma}(x,y), & \text{if } \gamma_{p-\theta_\sigma}(s) \geq \gamma_{p-\theta_\sigma}\big(\omega_{2,p-\theta_\sigma}(x,y)\big) \\ & \text{or } \omega_{2,p-\theta_\sigma}(x,y) < 0, \\ \omega_{2,p-\theta_\sigma}(x,y), & \text{otherwise.} \end{cases} \tag{15}$$

where the expression for $\alpha_{p-\theta_\sigma}(y)$ is given in (39) (see Appendix), $\gamma_{p-\theta_\sigma}(s)$ has to be replaced by the boundary data measured from the corresponding voltage field intensity (see (10)) and, the functions $\omega_{1,p-\theta_\sigma}(x,y)$ and $\omega_{2,p-\theta_\sigma}(x,y)$ are defined in (42) and (43) respectively (Appendix). The subscript, $p-\theta_\sigma$, of all the above functions indicates that the expressions of these functions change with the angle between the input current diameter and the flaw site. Note that $\lambda_{p-\theta_\sigma}(\cdot)$ is a lower-bound generator by Lemma10. $\omega_{p-\theta_\sigma}(\cdot,\cdot)$ is an upper-bound generator due to Lemma 14. Also, it is easy to show that $\lambda_{p-\theta_\sigma}(y)$ is decreasing with y on the interval $[0,2)$ for any fixed p and θ_σ.

The formulas (33)-(43) given in the appendix have to be stored in the algorithm before performing iteration. These formulas are algebraic functions without any integral expression involved. So the

computations of these functions are elementary and therefore the computational cost is low. Now, we state the iteration procedure to determine crack length.

Length algorithm ($r =$ *the radius of* Ω, $s = \frac{\ell_\sigma}{r}$) :

$$\left\{\begin{array}{ll} \text{Set} & s_0 = \dfrac{\text{radial damage size growth limit}}{r} \text{ or any} \\ & \qquad \text{possible upper bound of } s \\ & t_0 = \lambda_{p-\theta_\sigma}(s_0). \\ \text{For} & j = 0, 1, 2, 3, \ldots, \\ & s_{j+1} = \omega_{p-\theta_\sigma}(t_j, s_j), \\ & t_{j+1} = \lambda_{p-\theta_\sigma}(s_{j+1}). \end{array}\right\} \tag{16}$$

Terminate the iterations when $|s_j - s_{j-1}|$ *is within the required tolerance for some* j. *Let* ℓ_{app} *denote the approximate crack length. Then take*

$$\ell_{app} = r \times s_j \,.$$

The following result simply states that the above numerical iteration is convergent. This major feature of our length algorithm ensures the accuracy of an approximation to crack length within a required precision.

THEOREM 3.10. (Convergence of the length determination algorithm). *Two sequences* $\{s_j\}_{j=1}^{\infty}$ *and* $\{t_j\}_{j=1}^{\infty}$ *are constructed by the algorithm (16). Then*

$$0 < t_0 < t_1 < t_2 < \cdots < s < \cdots < s_2 < s_1 < s_0, \tag{17}$$

and

$$s_j \to s \quad \text{as} \quad j \to \infty. \tag{18}$$

The proofs of Theorem 3.10 will be divided into two stages. That is, we will verify (17) and (18) separately.

Proof of (17) we first claim that

$$0 < t_j < s < s_j < s_b, \qquad \forall j = 0, 1, 2, \ldots \tag{19}$$

This can be justified by induction. When $j = 0$, it is trivial from the length algorithm that $s < s_0 = s_b$. Applying Lemma 3.6, we have

$$\begin{aligned} s &> 2\sqrt{\frac{\gamma_{p-\theta_\sigma}(s)-1}{\alpha_{p-\theta_\sigma}(s_0)}}\Bigg/\left(1+\sqrt{\frac{\gamma_{p-\theta_\sigma}(s)-1}{\alpha_{p-\theta_\sigma}(s_0)}}\right) \\ &= \lambda_{p-\theta_\sigma}(s_0) = t_0. \end{aligned}$$

therefore (19) holds for $j = 0$. Assume (19) is valid for $j \le k$. That is,

$$0 < t_k < s < s_k < s_b.$$

Then by Lemma 3.9,

$$s < \omega_{1,p-\theta_\sigma}(t_k, s_k) < s_k \tag{20}$$

if $\gamma_{p-\theta_\sigma}(s) \ge \gamma_{p-\theta_\sigma}\big(\omega_{2,p-\theta_\sigma}(t_k, s_k)\big)$ or $\omega_{2,p-\theta_\sigma}(t_k, s_k) < 0$. Otherwise,

$$s < \omega_{2,p-\theta_\sigma}(t_k, s_k) < s_k \tag{21}$$

if $\omega_{2,p-\theta_\sigma}(t_k, s_k) \ge 0$ and $\gamma_{p-\theta_\sigma}(s) < \gamma_{p-\theta_\sigma}\big(\omega_{2,p-\theta_\sigma}(t_k, s_k)\big)$, since $\gamma_{p-\theta_\sigma}(\cdot)$ is increasing on $[0, 2)$. The second inequality in (21) is trivial from the definition of $\omega_{2,p-\theta_\sigma}$. (20) and (21) simply means

$$s < \underbrace{\omega_{p-\theta_\sigma}(\theta_\sigma, t_k, s_k)}_{s_{k+1}} < s_k. \tag{22}$$

Applying Lemma 3.6 under the condition (22) with the new upper bound s_{k+1} for s, it follows that

$$\begin{aligned} s &> 2\sqrt{\frac{\gamma_{p-\theta_\sigma}(s)-1}{\alpha_{p-\theta_\sigma}(s_{k+1})}}\Bigg/\left(1+\sqrt{\frac{\gamma_{p-\theta_\sigma}(s)-1}{\alpha_{p-\theta_\sigma}(s_{k+1})}}\right) \\ &= \lambda_{p-\theta_\sigma}(s_{k+1}) = t_{k+1} > 0. \end{aligned} \tag{23}$$

Coupling (22) and (23) together, we obtain (19) for $j = k + 1$. Therefore by induction, we have shown that (19) holds for all $j = 0, 1, 2, \ldots$.

At the same time, we have also proved that (22) is true for all $k = 0, 1, 2, \ldots$, i.e.,

$$s < \cdots < s_2 < s_1 < s_0 = s_b. \tag{24}$$

To complete the proof of (17), it remains to argue that $\{t_j\}_{j=0}^{\infty}$ is an increasing sequence. Since $\lambda_{p-\theta_\sigma}(\cdot)$ is decreasing on $[0,2)$ and $\{s_j\}_{j=0}^{\infty}$ is a decreasing sequence, (by (24)), we end up with

$$\lambda_{p-\theta_\sigma}(s_k) < \lambda_{p-\theta_\sigma}(s_{k+1}), \quad \forall\, k = 0,1,2,\ldots,$$

or equivalently,

$$t_k < t_{k+1}, \quad \forall\, k = 0,1,2,\ldots$$

So $\{t_j\}_{j=0}^{\infty}$ is an increasing sequence and (17) follows immediately. □

To complete the proof of Theorem 3.10, we need the following Lemma.

LEMMA 3.11.

$$\omega_{p-\theta_\sigma}(t_j, s_j) = \omega_{1,p-\theta_\sigma}(t_j, s_j), \quad \forall\, j \geq n_0 \text{ for some } n_0 \in \mathbb{N}.$$

Proof. Suppose this is not true, then from the definition of $\omega_{p-\theta_\sigma}$ given in (15), there must exist a subsequence $\{j_k\}_{k=1}^{\infty}$, such that

$$\omega_{p-\theta_\sigma}(t_{j_k}, s_{j_k}) = \omega_{2,p-\theta_\sigma}(t_{j_k}, s_{j_k}), \quad \forall\, k = 1,2,\ldots.$$

Since $\{t_j\}$ and $\{s_j\}$ are monotone bounded sequences, hence $\exists\ t^*$ and s^*, such that

$$t^* = \lim_{j\to\infty} t_j = \sup_j t_j, \quad \text{and} \quad s^* = \lim_{j\to\infty} s_j = \inf_j s_j. \tag{25}$$

Also we have

$$s_{j_k+1} - s = \omega_{2,p-\theta_\sigma}(t_{j_k}, s_{j_k}) - s = (s_{j_k} - s) + \\ - \min\left\{ \frac{A_{p-\theta_\sigma}(s_{j_k})}{\phi_{1,p-\theta_\sigma}(t_{j_k}, s_{j_k})}, \frac{B_{p-\theta_\sigma}(s_{j_k})}{\phi_{2,p-\theta_\sigma}(t_{j_k}, s_{j_k})}, \frac{C_{p-\theta_\sigma}(s_{j_k})}{\phi_{3,p-\theta_\sigma}(t_{j_k}, s_{j_k})} \right\}. \tag{26}$$

Note that $A_{p-\theta_\sigma}(\cdot)$, $B_{p-\theta_\sigma}(\cdot)$, and $C_{p-\theta_\sigma}(\cdot)$ are continuous on $[0,2)$. Each $\phi_{j,p-\theta_\sigma}(\cdot,\cdot)$ $(j = 1,2,3)$ is continuous on $[0,2)\times[0,2)$. (25) implies $\lim_{k\to\infty} s_{j_k} = s^*$ and $\lim_{k\to\infty} t_{j_k} = t^*$, passing limits on both sides of (26) as $k \to \infty$, we obtain

$$s^* - s = \\ (s^* - s) - \min\left\{ \frac{A_{p-\theta_\sigma}(s^*)}{\phi_{1,p-\theta_\sigma}(t^*, s^*)}, \frac{B_{p-\theta_\sigma}(s^*)}{\phi_{2,p-\theta_\sigma}(t^*, s^*)}, \frac{C_{p-\theta_\sigma}(s^*)}{\phi_{3,p-\theta_\sigma}(t^*, s^*)} \right\}.$$

Therefore from the above equation, it follows that

$$0 = \min\left\{\frac{A_{p-\theta_\sigma}(s^*)}{\phi_{1,p-\theta_\sigma}(t^*,s^*)}, \frac{B_{p-\theta_\sigma}(s^*)}{\phi_{2,p-\theta_\sigma}(t^*,s^*)}, \frac{C_{p-\theta_\sigma}(s^*)}{\phi_{3,p-\theta_\sigma}(t^*,s^*)}\right\}. \quad (27)$$

However, we have shown that

$$\gamma_{p-\theta_\sigma}(s^*) = A_{p-\theta_\sigma}(s^*)\cdot B_{p-\theta_\sigma}(s^*)\cdot C_{p-\theta_\sigma}(s^*)\cdot D_{p-\theta_\sigma} \geq 1, \quad (28)$$

and this implies that all of $A_{p-\theta_\sigma}(s^*)$, $B_{p-\theta_\sigma}(s^*)$ and $C_{p-\theta_\sigma}(s^*)$ must be greater than 0. Since each $\phi_{j,p-\theta_\sigma}(t^*,s^*)$ is nonnegative, we must have

$$0 < \min\left\{\frac{A_{p-\theta_\sigma}(s^*)}{\phi_{1,p-\theta_\sigma}(t^*,s^*)}, \frac{B_{p-\theta_\sigma}(s^*)}{\phi_{2,p-\theta_\sigma}(t^*,s^*)}, \frac{C_{p-\theta_\sigma}(s^*)}{\phi_{3,p-\theta_\sigma}(t^*,s^*)}\right\}.$$

But the last inequality contradicts (27). Therefore, there must exist an $n_0 \in \mathbb{N}$ so that

$$\omega_{p-\theta_\sigma}(t_j,s_j) = \omega_{1,p-\theta_\sigma}(t_j,s_j), \quad \forall\, j \geq n_0 \text{ for some } n_0 \in \mathbb{N}.$$

□

Finally, we show that the upper-bound sequence $\{s_j\}$ converges to the relative crack length, s. Then the proof for Theorem 3.10 is complete.

Proof of (18) By Lemma 3.11 and applying the formula (15), there must exist an $n_0 \in \mathbb{N}$ so that, $\forall j \geq n_0$

$$\begin{aligned} &s_{j+1} - s = \omega_{p-\theta_\sigma}(t_j,s_j) - s = \omega_{1,p-\theta_\sigma}(t_j,s_j) - s \\ &\leq (s_j - s) - \min\left\{\frac{\gamma_{p-\theta_\sigma}(s_j) - \gamma_{p-\theta_\sigma}(s)}{\beta_{p-\theta_\sigma}(t_j,s_j)}, \sqrt[3]{\frac{\gamma_{p-\theta_\sigma}(s_j) - \gamma_{p-\theta_\sigma}(s)}{\beta_{p-\theta_\sigma}(t_j,s_j)}}\right\}. \end{aligned}$$

Since $\gamma_{p-\theta_\sigma}(\cdot)$ is continuous on $[0,2)$ and $\beta_{p-\theta_\sigma}(\cdot,\cdot)$ is continuous on $[0,2)\times[0,2)$, taking limits as $j \to \infty$ on both sides of the above inequality and applying (25), we obtain

$$\begin{aligned} &s^* - s \leq \\ &\quad (s^* - s) - \min\left\{\frac{\gamma_{p-\theta_\sigma}(s^*) - \gamma_{p-\theta_\sigma}(s)}{\beta_{p-\theta_\sigma}(t^*,s^*)}, \sqrt[3]{\frac{\gamma_{p-\theta_\sigma}(s^*) - \gamma_{p-\theta_\sigma}(s)}{\beta_{p-\theta_\sigma}(t^*,s^*)}}\right\}. \end{aligned}$$

Therefore,

$$0 \geq \min\left\{ \frac{\gamma_{p-\theta_\sigma}(s^*) - \gamma_{p-\theta_\sigma}(s)}{\beta_{p-\theta_\sigma}(t^*, s^*)}, \sqrt[3]{\frac{\gamma_{p-\theta_\sigma}(s^*) - \gamma_{p-\theta_\sigma}(s)}{\beta_{p-\theta_\sigma}(t^*, s^*)}} \right\}. \quad (29)$$

Moreover, (17) and (25) implies $0 < t^* \leq s \leq s^* < 2$ and it follows that

$$\gamma_{p-\theta_\sigma}(s^*) - \gamma_{p-\theta_\sigma}(s) \geq 0 \quad (30)$$

because $\gamma_{p-\theta_\sigma}(\cdot)$ is increasing on $[0, 2)$. But (29) and (30) also gives us the following result,

$$\gamma_{p-\theta_\sigma}(s^*) - \gamma_{p-\theta_\sigma}(s) = 0 \quad (31)$$

since $\beta_{p-\theta_\sigma}(t^*, s^*) > 0$. Due to monotonicity of $\gamma_{p-\theta_\sigma}$, we conclude that $s = s^*$ from (31). That is, $\lim_{j\to\infty} s_j = s$. We have verified (18). □

REMARK 3.12. In this section, we assume that $0° < p - \theta_\sigma < 90°$ in our algorithm to determine the crack length ℓ_σ. This is exactly to avoid the extremal cases, *i.e.*, $p = \theta_\sigma$ or $p - \theta_\sigma = 90°$. As we have mentioned at the Remark 3.4, once we know the exact location of the exterior crack tip, we just need to fix a tiny angle ϕ so that $|p - \theta_\sigma| = \phi$ and go through the numerical experiment to determine ℓ_σ. See [6] for details.

4. Summary

We developed a reconstruction model to determine a surface crack from steady-state voltage boundary measurements. The shape of the crack is assumed to be linear. The detection method we proposed here was developed in the case of a planar circular domain . Employing the concept that we can transform any simply connected domain to the crack domain of our model via an analytic mapping, the method is also applicable to determine a surface crack in a $2D$ region of more complicate geometry. Our algorithms have the following merits:

(1) The method relies on only a finite number of boundary data.

(2) We can locate the exterior tip of a surface crack on the boundary.

(3) All the numerical algorithms in our detection procedure are easy to follow. They consist of only algebraic functions. So the computerized operations are elementary.

(4) The detection algorithms are convergent in determining the location and the length of a surface crack. The numerical results in [6, 19] indicate that our method is fast, stable and at low-cost for practice.

To test the algorithms, we conduct tremendous amount of numerical experiments. The reader is referred to another paper [6], where we also have detailed discussion about the sensitivity property of the method.

5. Appendix

In this section we provide a list of functions which have to be stored in the length algorithm. All these functions are algebraic and elementary. Hence the computational cost for these functions is lower compared with that for integral formulas.

$$\gamma_{p-\theta_\sigma}(s) =$$

$$\left|\frac{\tan\left(\frac{m-\theta_\sigma}{2}\right)\sec^2\left(\frac{m-\theta_\sigma}{2}\right)}{\tan\left(\frac{m_\sigma-\theta_\sigma}{2}\right)\sec^2\left(\frac{m_\sigma-\theta_\sigma}{2}\right)}\right| \times \frac{\left[\left(\frac{s}{2-s}\right)^2+\tan^2\left(\frac{m_\sigma-\theta_\sigma}{2}\right)\right]^{1/2}}{\left[\left(\frac{s}{2-s}\right)^2+\tan^2\left(\frac{m-\theta_\sigma}{2}\right)\right]^{1/2}}\times$$

$$\frac{\left[\left(\frac{s}{2-s}\right)^2+\tan^2\left(\frac{m_\sigma-\theta_\sigma}{2}\right)\right]^{1/2}+\left[\left(\frac{s}{2-s}\right)^2+\tan^2\left(\frac{p-\theta_\sigma}{2}\right)\right]^{1/2}}{\left[\left(\frac{s}{2-s}\right)^2+\tan^2\left(\frac{m-\theta_\sigma}{2}\right)\right]^{1/2}-\left[\left(\frac{s}{2-s}\right)^2+\tan^2\left(\frac{p-\theta_\sigma}{2}\right)\right]^{1/2}}\times$$

$$\frac{\left[\left(\frac{s}{2-s}\right)^2+\tan^2\left(\frac{m_\sigma-\theta_\sigma}{2}\right)\right]^{1/2}-\left[\left(\frac{s}{2-s}\right)^2+\tan^2\left(\frac{q-\theta_\sigma}{2}\right)\right]^{1/2}}{\left[\left(\frac{s}{2-s}\right)^2+\tan^2\left(\frac{m-\theta_\sigma}{2}\right)\right]^{1/2}+\left[\left(\frac{s}{2-s}\right)^2+\tan^2\left(\frac{q-\theta_\sigma}{2}\right)\right]^{1/2}}, \tag{32}$$

for $0^\circ < p - \theta_\sigma < 90^\circ$. where p, q, m, m_σ, and θ_σ in the above expression are measured in radiants rather than in degrees.

$$K_s(x) := \left[\left(\frac{s}{2-s} \right)^2 + \tan^2 \left(\frac{x}{2} \right) \right]^{1/2}. \tag{33}$$

$$A_{p-\theta_\sigma}(y) = \left| K_y(m_\sigma - \theta_\sigma) \cdot [K_y(m_\sigma - \theta_\sigma) - K_y(q - \theta_\sigma)] \right|, \tag{34}$$

$$B_{p-\theta_\sigma}(y) = \left| \frac{K_y(m_\sigma - \theta_\sigma) + K_y(p - \theta_\sigma)}{K_y(m - \theta_\sigma) + K_y(q - \theta_\sigma)} \right|, \tag{35}$$

$$C_{p-\theta_\sigma}(y) = \left| \frac{1}{K_y(m - \theta_\sigma)[K_y(m - \theta_\sigma) - K_y(p - \theta_\sigma)]} \right|, \tag{36}$$

$$D_{p-\theta_\sigma} = \frac{K_0(m - \theta_\sigma)[K_0^2(m - \theta_\sigma) + 1]}{K_0(m_\sigma - \theta_\sigma)[K_0^2(m_\sigma - \theta_\sigma) + 1]}, \tag{37}$$

$$\begin{cases} \psi_{1,p-\theta_\sigma}(x) = \dfrac{[K_x(q - \theta) - K_x(m_\sigma - \theta)]^2}{K_x(m_\sigma - \theta) K_x(q - \theta)}, \\ \psi_{2,p-\theta_\sigma}(x,y) = \dfrac{K_y(m_\sigma - \theta) + K_y(p - \theta)}{K_y(m - \theta) + K_y(q - \theta)} \times \\ \qquad \times \left[\dfrac{1}{K_x(m_\sigma - \theta) K_x(p - \theta)} - \dfrac{1}{K_x(m - \theta) K_x(q - \theta)} \right], \\ \psi_{3,p-\theta_\sigma}(x) = \dfrac{1}{K_x^3(m - \theta) K_x(p - \theta)}. \end{cases} \tag{38}$$

$$\begin{aligned} \alpha_{p-\theta_\sigma}(y) = {} & \tfrac{2\, D_{p-\theta_\sigma}}{2-y} \times \big[B_{p-\theta_\sigma}(0)\, C_{p-\theta_\sigma}(0)\, \psi_{1,p-\theta_\sigma}(0) + \\ & + A_{p-\theta_\sigma}(0)\, C_{p-\theta_\sigma}(0)\, \psi_{2,p-\theta_\sigma}(0,y) + \\ & + A_{p-\theta_\sigma}(0)\, B_{p-\theta_\sigma}(0)\, \psi_{3,p-\theta_\sigma}(0) \big] + \\ & + \tfrac{4y^2\, D_{p-\theta_\sigma}}{(2-y)^4} \times \big[C_{p-\theta_\sigma}(0)\, \psi_{1,p-\theta_\sigma}(0)\, \psi_{2,p-\theta_\sigma}(0,y) + \\ & + A_{p-\theta_\sigma}(0)\, \psi_{2,p-\theta_\sigma}(0,y)\, \psi_{3,p-\theta_\sigma}(0) + \\ & + B_{p-\theta_\sigma}(0)\, \psi_{1,p-\theta_\sigma}(0)\, \psi_{3,p-\theta_\sigma}(0) \big] + \\ & + \tfrac{8y^4\, D_{p-\theta_\sigma}}{(2-y)^7} \times \psi_{1,p-\theta_\sigma}(0)\, \psi_{2,p-\theta_\sigma}(0,y)\, \psi_{3,p-\theta_\sigma}(0). \end{aligned} \tag{39}$$

$$\begin{cases} \phi_{1,p-\theta_\sigma}(x,y) = \frac{2y}{(2-y)^3} \times \psi_{1,p-\theta_\sigma}(x), \\ \phi_{2,p-\theta_\sigma}(x,y) = \frac{2y}{(2-y)^3} \times \psi_{2,p-\theta_\sigma}(x,y), \\ \phi_{3,p-\theta_\sigma}(x,y) = \frac{2y}{(2-y)^3} \times \psi_{3,p-\theta_\sigma}(x), \end{cases} \tag{40}$$

$$\begin{aligned} \beta_{p-\theta_\sigma}(x,y) \;=\; & D_{p-\theta_\sigma}\big[B_{p-\theta_\sigma}(y)\, C_{p-\theta_\sigma}(y)\, \phi_{1,p-\theta_\sigma}(x,y) + \\ & + A_{p-\theta_\sigma}(y)\, C_{p-\theta_\sigma}(y)\, \phi_{2,p-\theta_\sigma}(x,y) + \\ & + A_{p-\theta_\sigma}(y)\, B_{p-\theta_\sigma}(y)\, \phi_{3,p-\theta_\sigma}(x,y) + \\ & + \phi_{1,p-\theta_\sigma}(x,y)\, \phi_{2,p-\theta_\sigma}(x,y)\, \phi_{3,p-\theta_\sigma}(x,y)\big]. \end{aligned} \tag{41}$$

$$\begin{aligned} &\omega_{1,p-\theta_\sigma}(x,y) = \\ &\max\left\{ \min\left\{ y - \frac{\gamma_{p-\theta_\sigma}(y) - \gamma_{p-\theta_\sigma}(s)}{\beta_{p-\theta_\sigma}(x,y)},\; y - \frac{\gamma_{p-\theta_\sigma}(y) - \gamma_{p-\theta_\sigma}(s)}{\beta_{p-\theta_\sigma}(\tilde{x},y)} \right\}, \right. \\ &\qquad \left. \min\left\{ y-1,\; y - \sqrt[3]{\frac{\gamma_{p-\theta_\sigma}(y) - \gamma_{p-\theta_\sigma}(s)}{\beta_{p-\theta_\sigma}(x,y)}} \right\} \right\}, \end{aligned} \tag{42}$$

$$\begin{aligned} &\omega_{2,p-\theta_\sigma}(x,y) = \\ &\max\left\{ y - \frac{A_{p-\theta_\sigma}(y)}{\phi_{1,p-\theta_\sigma}(x,y)},\; y - \frac{B_{p-\theta_\sigma}(y)}{\phi_{2,p-\theta_\sigma}(x,y)},\; y - \frac{C_{p-\theta_\sigma}(y)}{\phi_{3,p-\theta_\sigma}(x,y)} \right\}, \end{aligned} \tag{43}$$

where $\tilde{x} = \max(x, y-1)$, $\gamma_{p-\theta_\sigma}(y)$ is calculated using the formula, (32), and $\gamma_{p-\theta_\sigma}(s)$ is to be substituted by the boundary data (12).

References

[1] Alessandrini G., *Stable determination of conductivity by boundary measurements*, Appl. Anal. **27** (1988), 153–172.

[2] Alessandrini G., *Stable determination of a crack from boundary measurements*, Proc. Royal Soc. Edinb. Ser A **123**, No. 3 (1993), 497–516.

[3] ANDRIEUX S. and BEN ABDA A., *Identification of planar cracks by complete overdetermined data: inversion formulae*, Inverse Problems **12** (1996), 553–563.

[4] ALESSANDRINI G., BERETTA, E. and VESSELLA S., *Determining linear cracks by boundary measurements – Lipschitz stability*, SIAM J. Math. Anal., to appear.

[5] BRAY D. and STANLEY R., *Nondestructive evaluation: a tool for design, manufacturing and service*, McGraw-Hill, New York, 1989.

[6] BERENSTEIN C., CHANG D.C. and WANG E., *Determining a surface breaking crack from steady-state electrical boundary measurements – Numerical results*, Inverse Problems in Engineering **5** (1997), 279–308.

[7] BRYAN K., LIEPA, V. and VOGELIUS M., *Crack determination from boundary measurements*, Inverse Problems and Optimal Design in Industry, H. Engl and J. Mclaughlin eds., Teubner, Stuttgart.

[8] BRYAN K. and VOGELIUS M., *A uniqueness result concerning the identification of a collection of cracks from finitely many electrostatic boundary measurements*, SIAM J. Math. Anal. **23**, No. 4 (1992), 950–958.

[9] BRYAN K. and VOGELIUS M., *A computational algorithm to Determine crack locations from electrostatic boundary measurements. The case of multiple cracks*, Int. J. Engng Sci. **32** , No. 4 (1994), 579–603.

[10] ELCRAT A.R. and HU C., *Determination of surface and interior cracks from electrostatic measurements using Schwarz-Christoffel transformations*, Int. J. Eng. Science, to appear.

[11] ELCRAT A.R., ISAKOV V. and NECULOIU O., *On finding a surface crack from boundary measurements*, Inverse Problems **11** (1995), 343–352.

[12] FRIEDMAN A. and VOGELIUS M., *Determine cracks by boundary measurements*, Indiana Math. J. **38** (1989), 527–556.

[13] HALMSHAW R., "Nondestructive testing", Wiley-Intersciencs, New York, 1987.

[14] KAUP P.G. and SANTOSA F., *Nondestructive evaluation of corrosion damage using electrostatic measurements*, J. Nondestructive Evaluation, to appear.

[15] KAUP P.G., SANTOSA F. and VOGELIUS M., *A method for imaging corrosion damage in thin plates from electrostatic data*, Technical Report, CTC95TR219, Cornell Theory Center, Ithaca, 1995.

[16] LIEPA V., SANTOSA F. and VOGELIUS M., *Crack determination from boundary measurements-reconstruction from experimental data*, J. Nondestructive Evaluation **12** (1993), 163–173.

[17] MILITARY SPECIFICATION, *Airplane Damage Tolerance Requirements*, MIL-A-83444, USAF, 1974.

[18] SANTOSA F. and VOGELIUS M., *A computational algorithm to determine cracks from electrostatic boundary measurements*, Int. J. Engng Sci. **29**, No. 8 (1991), 917–937.

[19] WANG E., *Studies on an elliptic inverse boundary value problem and applications to defect determination*, Ph.D. thesis, University of Maryland, College Park, 1996

[20] WHEITNER J., *Investigation of the nondestructive evaluation of advanced materials: presented at the winter Annual Meeting of the American Society of Mechanical Engineers*, National Aeronautics and Space Administration, 1994.

Received September 5, 1997.